

Spectral measurements of hyper-Rayleigh light scattering

P. Kaatz and D. P. Shelton

Department of Physics, University of Nevada Las Vegas, Las Vegas, Nevada 89154-4002

(Received 16 October 1995; accepted for publication 2 January 1996)

An apparatus is described for the measurement of second-order nonlinear optical properties via hyper-Rayleigh scattering with 1 cm^{-1} spectral resolution of the scattered light. The setup allows a complete investigation of the polarization dependence of the second-harmonic scattered light. The combination of good spectral resolution, polarization analysis, and high sensitivity allows the determination of accurate polarization ratios of the scattered light. Consequently, information on the relative magnitude of hyperpolarizability components may be inferred from the measurements. Liquid phase measurements of a number of pure organic solvents including substituted benzene compounds are reported with approximately 5% uncertainty in the relative scattered intensities. Vapor phase measurements are also possible using the same apparatus, allowing a separation of the intrinsic molecular nonlinearities from contributions to hyper-Rayleigh scattering due to intermolecular interactions. © 1996 American Institute of Physics. [S0034-6748(96)02504-3]

I. INTRODUCTION

Several research groups have pointed out the advantages of using the hyper-Rayleigh light scattering (HRS) experiment to probe the second-order nonlinear optical response of molecules.¹⁻³ Until recently, the method of choice for measuring second-order nonlinear optical properties of organic molecules has been the electric-field-induced second-harmonic generation (EFISHG) experiment. As an external electric field is required in this experiment, only neutral dipolar molecules can be investigated for their nonlinear optical properties by the EFISHG experiment. In contrast, the HRS experiment requires only an efficient detection system to collect the scattered second-harmonic light. Consequently, HRS has been successfully used to measure the nonlinear optical properties of ionic species^{4,5} and octupolar molecules,^{6,7} in addition to the highly studied dipolar molecular compounds.^{3,8}

In molecular liquids, the second-harmonic scattered light can arise from both the intrinsic molecular properties and also from intermolecular interactions. As these effects typically have different spectral profiles, spectral resolution of the HRS signal enables one to perform a lineshape analysis of the scattered light in order to assess the various contributions to the HRS signal.⁹ Furthermore, as all components of the hyperpolarizability tensor can contribute to HRS, detailed polarization studies of the sample are needed in order to dissect the contributions of each component. The apparatus in general use for doing these experiments does not provide any detailed spectral information, as the spectral selectivity is achieved with interference filters.^{1-3,10-12} A few experiments have been reported on the hyper-Raman and/or hyper-Rayleigh spectra of selected molecules with spectral resolution of $\approx 1\text{ cm}^{-1}$.¹³⁻¹⁵ In these experiments, however, the authors did not investigate the polarization dependence of the HRS signal nor was there any calibration of the intensity of the scattered light.

The apparatus described in this work provides 1 cm^{-1} resolution of the scattered light and the ability to study the full polarization dependence of the sample. Both liquid and

gas phase measurements are possible with this apparatus, which aids in separation of the molecular and intermolecular contributions to the HRS signal. We derive expressions which relate the nonlinear optical properties of molecules to the measured HRS signals. The low power, high repetition rate laser source, and high efficiency detection system allow the measurement of the polarized HRS spectra of a number of organic liquids including substituted benzene compounds.

II. THEORY

When a molecule is irradiated with light of high intensity, the resulting nonlinear optical response is usually written as a Taylor series expansion of the induced dipole moment μ in terms of the applied electric field $E_i(\omega)$ as

$$\mu_i = \alpha_{ij}E_j + \frac{1}{2}\beta_{ijk}E_iE_j + \dots, \quad (1)$$

where the molecular tensors α and β describe the linear and lowest-order nonlinear optical properties of the molecules, respectively. If the incident light is assumed to be travelling in the x direction, as in Fig. 1, the polarization of the incident electric field, $\mathbf{E}(\omega)$, can be described by

$$\mathbf{E}(\omega) = E_0[\cos\psi\cos\omega t\mathbf{e}_y + \sin\psi\cos(\omega t + \delta)\mathbf{e}_z], \quad (2)$$

where ψ and δ are arbitrary angles. Circularly polarized light is described by $\psi = \pi/4$ and $\delta = \pi/2$ and linearly polarized light by $\psi = 0$ (horizontal) or $\psi = \pi/2$ (vertical).

The second-harmonic light intensity for a collection of N incoherently scattering molecules is, $I^{2\omega} \propto N\langle\mu_i(2\omega)\mu_i^*(2\omega)\rangle$, where $\mu_i(2\omega)$ is the induced dipole moment for a single molecule. The time averaging over the motions of the molecules indicated by the brackets will involve products of components of the first hyperpolarizability tensor β of the form $\langle\beta_{IJK}\beta_{LMN}\rangle$. Assuming the scattered HRS signal is collected at 90° along the y direction, the polarization dependence of the second-harmonic signal is given by¹⁶

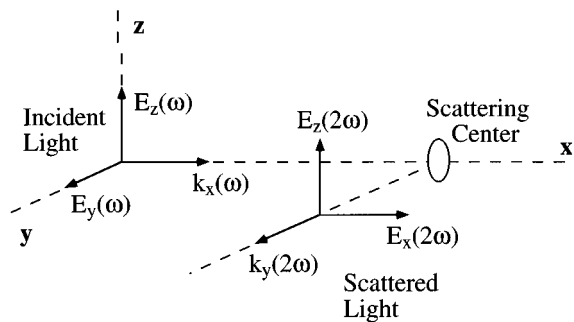


FIG. 1. Propagation and polarization directions of the incident fundamental and scattered second-harmonic radiation field.

$$I_{EH}^{2\omega} \propto \langle \mu_x^2 \rangle \propto \langle \beta_{XZZ}^2 \rangle \sin^4 \psi + \langle \beta_{XY Y}^2 \rangle \cos^4 \psi + \sin^2 \psi \cos^2 \psi \langle (\beta_{XYZ} + \beta_{XZY})^2 + 2\beta_{XZZ}\beta_{XY Y} \cos 2\delta \rangle, \quad (3a)$$

$$I_{EV}^{2\omega} \propto \langle \mu_z^2 \rangle \propto \langle \beta_{ZY Y}^2 \rangle \cos^4 \psi + \langle \beta_{ZZZ}^2 \rangle \sin^4 \psi + \sin^2 \psi \cos^2 \psi \langle (\beta_{ZY Z} + \beta_{ZZY})^2 + 2\beta_{ZZZ}\beta_{ZY Y} \cos 2\delta \rangle, \quad (3b)$$

where the subscripts *V*, *H*, and *E* indicate vertically, horizontally, and elliptically polarized light, respectively. The macroscopic averages $\langle \beta_{IJK} \beta_{LMN} \rangle$ are quadratic forms of the microscopic molecular-fixed-axis hyperpolarizability components, β_{ijk} .^{16–18} In the general case, at most five invariants of the molecular hyperpolarizabilities may be determined, depending upon the molecular symmetry. The use of linearly and circularly polarized radiation allows the determination of three independent polarization ratios. Consequently, elliptically polarized light is required to obtain full information on these invariants when using Eqs. (3a) and (3b). It is sufficient to use incident light of various elliptical polarizations and a linear polarizer to analyze the scattered light, as this provides polarization ratios that are dependent upon all five invariants of the HRS experiment.

A Soleil–Babinet compensator is used in the apparatus described below to create elliptically polarized light from the incident horizontally or vertically polarized light. The compensator is characterized by an azimuth ϕ , which specifies the orientation of an optic axis with respect to the polarization of the incident light and Γ , the relative retardation between light waves traveling along the fast and slow axes of the compensator. If the azimuth of the compensator is set at $\phi=45^\circ$, the Jones matrix describing the compensator can be written as¹⁹

$$\begin{bmatrix} \cos \Gamma/2 & -i \sin \Gamma/2 \\ -i \sin \Gamma/2 & \cos \Gamma/2 \end{bmatrix}. \quad (4)$$

Using the Jones matrix in Eq. (4), with horizontally polarized light incident on the compensator, the polarization of the light leaving the compensator can be written as

$$\mathbf{E}(\omega) = E_0(\omega) \left(\cos \frac{\Gamma}{2} \mathbf{e}_H - i \sin \frac{\Gamma}{2} \mathbf{e}_V \right). \quad (5)$$

The polarization of the light leaving the compensator is equivalent to the polarized light described by Eq. (2) provided that $\delta=\pi/2$ and $\psi=\Gamma/2$. The standard *VV* and *VH* polarization geometries in Eqs. (3a) and (3b) correspond to setting the retardation of the compensator to $\Gamma=2\psi=\pi$, and selecting *V* or *H* with the appropriate setting of the analyzer. Similarly, the *HV* and *HH* scattering geometries are obtained from $\Gamma=2\psi=0$, with $\delta=\pi/2$ and the *V* or *H* setting of the analyzer.

Molecules of T_d symmetry have only one nonzero-independent hyperpolarizability component, β_{xyz} . For this symmetry group the intensities $I_{EV}^{2\omega}$ and $I_{EH}^{2\omega}$ given by Eqs. (3a) and (3b) simplify to

$$I_{\psi V}^{2\omega} \propto \langle \mu_z^2 \rangle \propto \frac{12}{35} \beta_{xyz}^2 \left(1 + \frac{5}{3} \cos^2 \psi - 2 \cos^4 \psi \right), \quad (6a)$$

$$I_{\psi H}^{2\omega} \propto \langle \mu_x^2 \rangle \propto \frac{8}{35} \beta_{xyz}^2 (1 + \cos^2 \psi - \cos^4 \psi) \quad (6b)$$

when δ is fixed at $\pi/2$. The same proportionality constant is used in Eqs. (6a), (6b) and (3a), (3b). For molecules of lower symmetry, the corresponding expressions will depend on several of the hyperpolarizability components, giving information on their relative magnitude.

Assuming the second-harmonic scattered light is broadened by rotational diffusion of the molecules, the spectral distribution of the second harmonic scattered light is a sum of Lorentzian line shapes.²⁰ Intermolecular interactions also broaden the spectral distribution, typically giving a component with an exponential profile.²¹ The experimental spectra were therefore fitted with the sum of a single Lorentzian of integrated intensity I_1 and an exponential with integrated intensity I_2 :

$$I_{VV}^{2\omega}(\Delta\nu) = \left[I_1 \frac{\nu_1/\pi}{\Delta\nu^2 + \nu_1^2} \left(\frac{2}{1 + \exp|\Delta\nu/\nu_0|} \right) + I_2 \frac{\exp - |\Delta\nu/\nu_2|}{2\nu_2} \right] \exp(-\Delta\nu/2kT). \quad (7)$$

The Lorentzian function in Eq. (7) has its far wings clipped; at large $|\Delta\nu|$ it becomes an exponential, as the Lorentzian becomes inappropriate at high frequencies since rotational diffusion does not describe the molecular motion on time scales smaller than the mean time between collisions. Typically ν_0 is approximately 50–100 cm^{-1} , corresponding to a collision interval of about 0.05–0.1 ps. The last exponential factor accounts for the Stokes/anti-Stokes asymmetry ($2kT=410 \text{ cm}^{-1}$ at 22 °C). All of the spectra measured in this work are adequately described by an expression of this form, as indicated by the case of chlorobenzene shown in Fig. 2. In general, a more complete analysis of the HRS spectra may require the use of multiple Lorentzians and/or exponential terms to correctly interpret the spectra.

III. EXPERIMENTAL APPARATUS

A. Laser system

Laser systems in current use for HRS measurements are primarily flashlamp pumped Nd:YAG lasers *Q*-switched by a

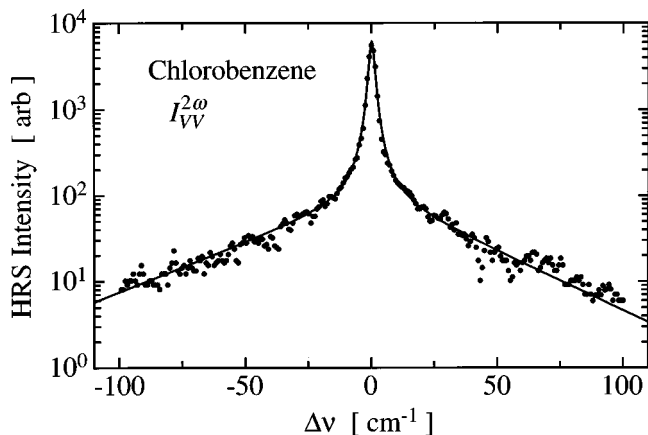


FIG. 2. $I_{VV}^{2\omega}$ HRS scattering from chlorobenzene at 22 °C with irradiation at 1064 nm. The Lorentzian term is fitted with $2\nu_1=2.4\pm 0.2\text{ cm}^{-1}$ and the exponential term with $\nu_2=35\pm 3\text{ cm}^{-1}$.

Pockel's cell.^{1-3,10} Although these lasers provide the high intensity needed to generate second-harmonic light, the Q -switch frequency is limited to frequencies $<100\text{ Hz}$. The use of a cw pumped acousto-optically Q -switched Nd:YAG laser provided repetition rates (1–50 kHz) that are more convenient for spectral studies of HRS. The experimental apparatus used in this work is shown schematically in Fig. 3. The source radiation at 1064 nm was obtained from a Quantronix 116 cw pumped Nd:YAG laser operating in a near Gaussian TEM₀₀ mode with a measured $M^2\approx 1.1$. The laser produced trains of $\approx 150\text{ ns}$, 1 mJ pulses at working repetition rates of 1–3 kHz. The input power level and polarization are selected by two Glan–Laser polarizers followed by a Soleil–Babinet compensator. The fast axis of the compensator is set at 45° with respect to the vertical axis, fixing δ at $\pi/2$. A visible blocking filter (RG 850) is placed in the final position before the focusing lens to prevent any second harmonic light that is generated in the laser path from entering the sample cell. The laser beam is focused into the sample cell with a 4× microscope objective lens (focal length 32 mm).

The measured beam waist diameter is 14 μm (confocal parameter $z_0=100\text{ }\mu\text{m}$), giving a peak intensity about 1 GW/cm^2 at the focus of a 1 kW beam. The intensity is much smaller at the windows, where the beam diameter is $\approx 0.5\text{ mm}$. The choice of the degree of focusing is not critical since the signal from a given sample is actually independent of the degree of focusing provided light is collected from the entire

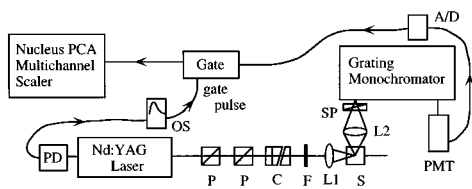


FIG. 3. Experimental setup for spectral measurements of hyper-Rayleigh light scattering. The components are denoted by: P: Glan-laser polarizer; C: Soleil–Babinet compensator; F: RG 850 filter; L1: 4× microscope objective; L2: 50 mm camera lens; PD: photodiode; S: sample cell; SP: sheet polarizer; OS: oscilloscope; PMT: photomultiplier tube; A/D: amplifier/discriminator.

beam length and the beam is nearly diffraction limited (signal $\propto n/\lambda M^2$, where n is the sample refractive index). Since the scattering is strongly dependent on intensity, most of the light is produced near the focus, with 99% of the signal produced between $-3z_0 < z < 3z_0$. In our case this is a region of length 0.6 mm.

It is interesting to consider how the peak power of the laser pulses affects the form of the apparatus. The maximum intensity at the focus is set by the threshold for damage and undesired nonlinear effects. As the peak power increases, the beam must be focused more weakly so as not to exceed this maximum intensity ($z_0 \propto \text{peak power}$). Compared to our system with 150 ns, 1 mJ pulses at 3 kHz, a higher-power 10 Hz system with 15 ns, 1 mJ pulses will generate 10× as many second-harmonic photons per pulse but will require a 10× longer sample region. Since the pulse repetition rate in our system is 300× higher, our system will produce a 30× larger signal from a 10× smaller sample.

B. Sample preparation

A particular advantage of the present apparatus is the minimal amount of sample material needed for an HRS measurement. Normal 1 cm spectroscopic glass cuvettes are used for measurements of pure solvents or solutions, and in typical experiments a 1.0 cm^3 sample of liquid is sufficient. With other standard cuvettes the required sample volume could be reduced to $\approx 0.1\text{ cm}^3$. The liquids are filtered through a 0.2 μm micropore filter to remove dust particles that could be a source of SHG signal. Strong thermal lensing is observed for hydrogenated molecules due to absorption at 1064 nm by a C–H vibrational overtone, limiting the HRS signal as the beam is defocused at higher intensities. The thermal lensing disappears for fully deuterated compounds or ones without hydrogen, such as carbon tetrachloride, CCl_4 .

C. Photon collection and detection

The second-harmonic scattered light is collected at 90° with an $f/1.4$ camera lens and focused into a tandem grating spectrometer (Jobin–Yvon Ramanor U 1000). The polarization of the scattered light is analyzed with a sheet polaroid (transmission=77% and extinction ratio= 5×10^{-4} at $\lambda=532\text{ nm}$). The 50 mm focal length camera lens is mounted on precision translation stages and is positioned so that a 5× magnified image of the scattering region falls on the entrance slit of the spectrometer. Field lenses are used at the spectrometer entrance and exit slits to improve the transfer of light from off-center image points, through the spectrometer and to the photomultiplier tube. The optics collect light at $f/1.8$ from the sample and just fill the $f/9$ acceptance aperture of the spectrometer. The signal reduction due to the spectrometer is only a minor consideration since the transmission probability for a V polarized HRS photon entering the spectrometer is 30% at $\lambda=532\text{ nm}$, not much lower than the 35% transmission of a 3 nm bandpass interference filter. The entrance slit can be closed to a spectral slit width of 0.8 cm^{-1} (physical slit width 100 μm) before it begins to block light from the image of the scattering source. The liquid line-shape measurements were done with a spectral slit width

of 1.2 cm^{-1} . For vapor phase measurements the slits were opened to 13 cm^{-1} . The spectrally dispersed light was detected by a cooled photon-counting photomultiplier tube (Hamamatsu R943) followed by an amplifier/discriminator. The output pulses corresponding to individual detected photons are counted by a multichannel scaler (Nucleus PCA).

The polarization-dependent response of the detection system enters into the polarization analysis of the collected HRS light. The polarization ratio of the collected light (C) is related to the polarization ratio of the detected light (D) by

$$\left(\frac{I_{VV}}{I_{\psi V}}\right)_C = \left(\frac{I_{VV}}{I_{\psi V}}\right)_D \left\{ \left[1 + r s \left(\frac{I_{\psi H}}{I_{\psi V}}\right)_C \right] / \left[1 + r s \left(\frac{I_{VH}}{I_{VV}}\right)_C \right] \right\}, \quad (8a)$$

$$\left(\frac{I_{\psi V}}{I_{\psi H}}\right)_C = s \left(\frac{I_{\psi V}}{I_{\psi H}}\right)_D \left\{ \left[1 + \frac{r}{s} \left(\frac{I_{\psi V}}{I_{\psi H}}\right)_C \right] / \left[1 + r s \left(\frac{I_{\psi H}}{I_{\psi V}}\right)_C \right] \right\}, \quad (8b)$$

where $r = T_{A,\perp}/T_{A,\parallel}$ is the analyzer extinction ratio, and $s = T_{S,H}/T_{S,V}$ is the spectrometer transmission ratio for horizontally and vertically polarized light. For the ideal instrument $r=0$ and $s=1$. The value of s for the present spectrometer varies from 10 at $\lambda=450 \text{ nm}$ to 0.05 at 700 nm, and has a value of 0.20 at 532 nm. Since the ratio s enters as a leading factor in Eq. (8b), one must measure and correct for the polarization dependence of the spectrometer to correctly determine these polarization ratios. The other corrections in Eqs. (8) are small for $r < 10^{-3}$. If the polarizer axis is misaligned with the laser beam axis by an angle $\Delta\alpha$, then the effective extinction ratio is increased to $r_{\text{eff}} = r + \tan^2(\Delta\alpha)$.

As the optics collect light at $f/1.8$ from the scattering source, the polarization analysis of the HRS scattered light requires an averaging over angles around the nominal 90° scattering geometry. The spectra were corrected for the effect of a finite collection angle θ_0 by using

$$(I_{EH}^{2\omega})_C \propto AA \langle \mu_x^2 \rangle + BB \langle \mu_y^2 \rangle, \quad (9a)$$

$$(I_{EV}^{2\omega})_C \propto CC \langle \mu_x^2 \rangle + DD \langle \mu_y^2 \rangle + EE \langle \mu_z^2 \rangle, \quad (9b)$$

where the coefficients $AA-EE$ are averages over the collection aperture as given in Table I. In the ideal case ($\theta_0=0$), $AA=EE=1$ and $BB=CC=DD=0$, and Eqs. (9a) and (9b) reduce to Eqs. (3a) and (3b). For finite collection apertures, $AA \neq EE$, which implies that the scattering geometries VH and HV are not equivalent. At $f/1.8$, the corrections to $I_{VV}^{2\omega}/I_{VH}^{2\omega}$ are always less than 2%, but corrections to $I_{VV}^{2\omega}/I_{HV}^{2\omega}$ are as large as 15% when $I_{VV}^{2\omega}/I_{HV}^{2\omega}=10$. The size of the corrections scales as θ_0^2 and varies roughly linearly with the polarization ratio.

The correction for a finite collection angle also requires the orientational average $\langle \mu_y^2 \rangle$. In the general case, an expression can be written similar to Eqs. (3a) and (3b).¹⁶ For the case of T_d symmetry this expression simplifies to

$$\langle \mu_y^2 \rangle \propto \frac{8}{35} \beta_{xyz}^2 \left(1 + \frac{7}{2} \cos^2 \psi - 3 \cos^4 \psi \right), \quad (10)$$

where the proportionality factor is the same as in Eqs. (3) and (6). Equations (6), (9), (10) together with the tabulated values of the coefficients $AA-EE$ in Table I are sufficient to

TABLE I. The effect of a finite collection angle on the measured polarization ratios in the nominal 90° geometry is expressed by Eqs. (9) with coefficients AA, BB, \dots . The coefficients are obtained by averaging the corresponding angular functions over the collection aperture (the nominal observation direction is the polar axis and θ, ϕ are the usual spherical polar coordinates). The coefficients are subject to the constraints $AA+BB=1$ and $CC+DD+EE=1$. Numerical values are shown for two collection angles corresponding to $f/1.8$ and $f/3.0$.

Coefficient	Angular function	Ave. at $f/1.8$	Ave. at $f/3.0$
AA	$\frac{\cos^2 \theta}{1 - \sin^2 \theta \cos^2 \phi}$	0.98177	0.99320
BB	$\frac{\sin^2 \theta \sin^2 \phi}{1 - \sin^2 \theta \cos^2 \phi}$	0.01823	0.00680
CC	$\frac{\sin^4 \theta \sin^2 \phi \cos^2 \phi}{1 - \sin^2 \theta \cos^2 \phi}$	0.00022	0.000031
DD	$\frac{\sin^2 \theta \cos^2 \theta \cos^2 \phi}{1 - \sin^2 \theta \cos^2 \phi}$	0.01779	0.00674
EE	$1 - \sin^2 \theta \cos^2 \phi$	0.98199	0.99323

correct the measured polarization ratios for molecules of T_d symmetry. Corrections to measurements of molecules with other point groups are straightforward with the appropriate calculations of $\langle \mu_i^2 \rangle$.

A photodiode and oscilloscope monitor the laser output, and also generate a pulse which is used to open an electronic gate during the laser pulse. By accepting photon counts only during the laser pulse, the random background count rate is reduced by a factor of about 2000, giving a typical background count rate of 0.002 Hz. The typical HRS signal from a liquid sample is one photon counted per ten laser pulses, yielding an average signal count rate of 300 Hz. In some circumstances the HRS signal is much stronger and several scattered photons may be detected per laser pulse. The photons tend to be closely bunched near the peak of the laser pulse, and the pulse counting electronics are too slow to reliably count multiple photons detected during a single laser pulse. To avoid inaccurate results due to this problem, the electronics are set up to register only a count of either 0 or 1 during a laser pulse, and the true signal count-rate S^* is determined from the measured signal count-rate S by applying the following expression:²²

$$S^* = -R \ln(1 - S/R), \quad (11)$$

where R is the laser repetition rate and Poisson counting statistics are assumed. The most accurate results are obtained when S/R is small.

D. Vapor-liquid intensity comparison

The space above the liquid sample in a cuvette is filled with the vapor of the sample molecules. The scattering from the liquid and from the vapor can be compared by simply shifting the cuvette vertically a few mm so that the laser beam passes either through the liquid or just above the liquid surface. Compared with corresponding Rayleigh scattering ratio measurements, the HRS measurements have the advantage that they are insensitive to the strong background of laser light scattered without a frequency shift. However, there are still several serious difficulties in practice. The HRS

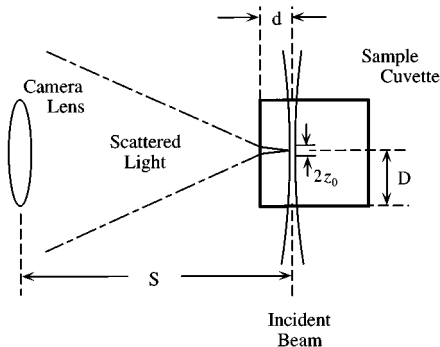


FIG. 4. Schematic diagram showing the configuration of the sample cell (1 cm cuvette), the focused incident beam, and the collection optics for the second-harmonic scattered light. The incident laser beam passes through the cell at distance $d \approx 1-2$ mm from the cell wall, with the focal point approximately in the center of the cell, $D \approx 5$ mm. The position S of the camera lens is optimized with the monochromator slits closed to $\approx 100 \mu\text{m}$ (spectral width $\approx 1 \text{ cm}^{-1}$). When the sample is changed, the focusing and collection lenses are moved by the distances given by Eqs. (12) and (13) to maintain the same optical path lengths and collection geometry.

signal from a vapor sample is about 10^4 times lower than that from the liquid. For example, with 2.5 W average laser power incident on a 300 Torr CCl_4 vapor sample (50°C), the typical HRS signal integrated over the entire spectrum is 0.3 counts per minute (the gated background dark count rate adds 0.1 cpm). This limits the signal/noise ratio that may be attained in a reasonable time, especially in spectral measurements. It is also extremely difficult to adjust the alignment of the apparatus using the signal from the vapor. Nevertheless, a valid comparison of liquid and vapor scattering intensities requires that the scattering and collection geometry be correctly set for both samples. Below we explain how this is achieved.

Figure 4 shows the optical arrangement around the sample cell in more detail. The effects of substituting vapor for liquid inside the sample cell are several. The first effect is that the focusing of the laser beam is modified. While the diffraction-limited spot size is the same in liquid and vapor, the confocal parameter z_0 is larger by a factor n_L/n_V in the liquid. To maintain the beam waist at the same position inside the cell (distance D from the inside face of the entrance window), the laser focusing lens is moved toward the sample cell a distance

$$\delta D = D(n_L - n_V)/n_L \quad (12)$$

when vapor replaces liquid. The focusing lens is mounted on a translation stage and is typically displaced 1.6 mm to keep the focus centered in the cell. Spherical aberration due to the slab of liquid in the focused beam causes a negligible systematic error, since it increases the effective spot size $< 0.5\%$ for an input beam diameter < 3 mm at the lens.

The second effect of replacing the liquid in the cell with vapor is that the apparent position of the scattering source seen by the collection optics changes, even though the focused laser beam passes through the sample cell at a fixed distance d behind the inside surface of the viewing window. The collection lens must be moved towards the cell by a distance

$$\delta S = d(n_L - n_V)/n_L \quad (13)$$

in order that the optical path length from scattering source to lens remains constant when vapor replaces liquid in the cell. In this way the magnification of the image formed by the lens remains constant, but the image is now formed a distance δS in front of the entrance slit of the spectrometer. However, there is no difference in the amount of light accepted by the spectrometer even though the incident light is slightly out of focus at the slit. Typically, $d = 1$ mm, $\delta S = 0.3$ mm, and magnification $M = 5$, so the image of the beam waist is $70 \mu\text{m}$ wide and the out-of-focus band of light at the plane of the entrance slit is $130 \mu\text{m}$ wide, much narrower than the 3 mm slit width used in these measurements. The slits are also much longer (25 mm) than the image of the scattering source. The image can be focused in the plane of the entrance slit by moving the lens slightly closer to the sample cell, but this is not desirable since then the amount of light that is collected and the fraction of the collected light that is coupled through the spectrometer both change by uncertain factors.

The third difference between liquid and vapor samples is that light is collected over a solid angle larger by a factor $(n_L/n_V)^2$ in the vapor. Fourth, the Fresnel transmission coefficients change at the inside surfaces of the entrance and viewing windows of the sample cell. The transmission coefficient is $T_{s,\omega} = [1 - (n_w - n_s)^2 / (n_w + n_s)^2]$, for window and sample refractive indices n_w and n_s at frequency ω , and $S = L$ or V . Fifth, the local fields at the sample molecules and the density of the sample molecules change. The Lorentz local field factor for sample S at frequency ω is $\mathcal{L}_{S,\omega} = (n_{S,\omega}^2 + 2)/3$. The vapor density is set by the saturated vapor pressure of the sample at the temperature of the sample cell. Provided the laser focusing lens and the light collection lens are repositioned according to Eqs. (12) and (13), the relation between the HRS signals from the liquid and vapor is given by

$$\frac{S_L}{S_V} = \frac{n_{L,\omega}}{n_{V,\omega}} \frac{n_{V,2\omega}^2}{n_{L,2\omega}^2} \frac{T_{L,\omega}^2 T_{L,2\omega}}{T_{V,\omega}^2 T_{V,2\omega}} \frac{\mathcal{L}_{L,\omega}^4 \mathcal{L}_{L,2\omega}^2 \rho_L \beta_L^2}{\mathcal{L}_{V,\omega}^4 \mathcal{L}_{V,2\omega}^2 \rho_V \beta_V^2}, \quad (14)$$

where the factors account for effective scattering source length, collection solid angle, reflection losses, local fields, sample density, and molecular hyperpolarizability, in that order. The same expression applies when comparing two different liquid samples. The change in signal when measuring the same chromophore in different solvents can be quite significant. For example, ignoring possible changes in the molecular hyperpolarizabilities, a $2.87 \times$ increase in the HRS signal is predicted by Eq. (14) when changing the solvent from ethanol to chloroform.

To test the experimental procedure, measurements were made of the ratio of scattered intensities for several Raman bands in CCl_4 liquid and vapor using a cw argon-ion laser at $\lambda = 488.0$ and 514.5 nm. The signal from the vapor is strong enough that the predicted focal shifts can be directly measured and verified. For Raman scattering the signal is linear in the laser beam intensity, so the relation analogous to Eq. (14) is

TABLE II. Measurements of the polarizations ratios, integrated intensities, and Lorentzian bandwidths of the HRS spectra for several liquids at 22 °C.

Liquid	$I_{VV}^{2\omega}/I_{HH}^{2\omega a}$	$I_{VV}^{2\omega}/I_{HV}^{2\omega b}$	$I_{VV}^{2\omega c}$	$2\nu_1$ (cm ⁻¹) ^d
Fused silica	1.56±0.05		0.072±0.003	<0.2 ^e
Carbon tetrachloride	1.81±0.05	1.54±0.05	1.0	9.2
Acetonitrile	10.2±0.3		1.7±0.1	4.2
Chloroform	3.1±0.2		0.70±0.05	4.8
Nitromethane	4.4±0.2		0.42±0.03	5.1
Pyridine	4.3±0.2		1.6±0.2	2.6
Chlorobenzene	4.3±0.2		1.3±0.1	2.4
Nitrobenzene	10.4±0.2		95±5	1.3
1,3,5 Trifluorobenzene	1.54±0.05	1.50±0.05	1.2±0.1	8.8

^aPolarization ratios measured at $\Delta\nu=0$ with a spectral slit width of 1.2 cm⁻¹, corrected for finite collection angle.

^bPolarization ratios calculated from the integrated Lorentzian contribution to the total HRS signal corrected for finite collection angle.

^cTotal integrated HRS signal relative to carbon tetrachloride.

^dFull width at half maximum (FWHM). Fits were made to the liquid spectra without deconvolving the 1.2 cm⁻¹ FWHM instrumental profile.

^eWidth obtained with 0.5 cm⁻¹ spectral slit width and deconvolution. The spectrum approximates a delta function.

$$\frac{S_L}{S_V} = \frac{n_V^2}{n_L^2} \frac{T_L^2}{T_V^2} \frac{\mathcal{L}_L^4}{\mathcal{L}_V^4} \frac{\rho_L}{\rho_V} \frac{\alpha_L^2}{\alpha_V^2}. \quad (15)$$

In Eq. (15), the distinction between incident and scattered frequency has been ignored. The Raman ratio measurements are not sensitive to small changes in laser beam spot size, but they do provide an effective test of the collection geometry. The measured ratios $(\alpha_L/\alpha_V)^2$ for the ν_1 , ν_2 , and ν_4 Raman bands of CCl₄ (at $\Delta\nu=459$, 214, and 314 cm⁻¹) are 0.90, 0.72, and 0.79, to be compared with the previously determined values 0.87, 0.78, and 0.77 at 514.5 nm.^{23,24} The agreement is satisfactory, and is consistent with an accuracy better than 5% for Raman or HRS liquid/vapor intensity ratio determinations with this apparatus. The measurement procedure is straightforward. The focusing and alignment is done with the laser beam passing through the liquid sample. The liquid signal is measured and then the sample cell is lowered so the beam passes through the vapor, the lenses are moved the calculated distances, and the vapor signal is measured. One may easily return to the liquid measurement configuration to check for drifts which may have occurred during the much longer vapor signal measurement.

IV. RESULTS AND DISCUSSION

Table II collects the results obtained for liquids measured using the apparatus described in this work. The measured polarization ratios and linewidths are in reasonable agreement with the results of Maker for the case of previously investigated molecules.²⁰ The relative intensity ratios in Table II have been corrected for the effects of thermal lensing by extrapolation to zero power as indicated for the case of acetonitrile in Fig. 5. The measured relative intensities are believed to be the only reported measurements of pure solvents done in direct comparison with each other and fused silica since the original work of Terhune *et al.* in 1965.²⁵ These ratios should resolve some problems with present HRS intensity comparisons. For example, current reported HRS intensity ratios for chloroform relative to carbon

tetrachloride vary over nearly a factor of 3, from 0.47 to 1.36.^{2,6} This is a problem since chloroform is widely used as a solvent and internal standard in HRS measurements. A possible source for such widely variable results in even this simple comparison of similar molecules may be two-photon fluorescence of the amylene inhibitor sometimes added to chloroform, since broadband fluorescence is only partially rejected by the interference filter in the usual apparatus. In other comparisons, the differences in the HRS polarization ratios for molecules of different symmetry may be important. In a typical application of the internal reference method, measurements for a series of solutions of a chromophore in a particular solvent are extrapolated to infinite dilution in order to determine the relative HRS intensities for the solvent and chromophore molecules. In the case where the symmetry of the chromophore and solvent molecules are different, and the measurements are done without the benefit of polarization analysis, the measured intensity ratios may be subject to

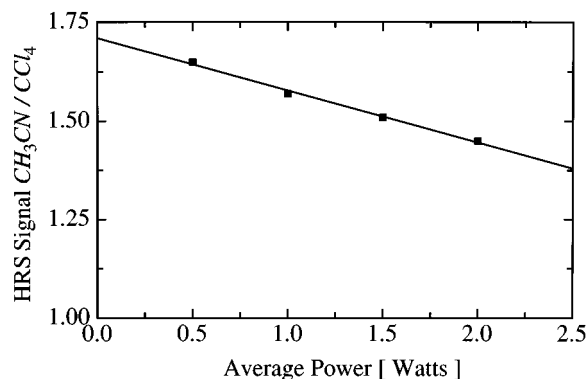


FIG. 5. Power dependence of the HRS $I_{VV}^{2\omega}$ signal from acetonitrile in comparison with the corresponding intensity from CCl₄. The laser was operating at a repetition rate of 3 kHz with pulse widths of ≈ 150 ns and pulse energies of ≈ 0.1 –1.0 mJ. Due to absorption at 1064 nm by a C–H vibrational overtone, the beam is defocused at higher intensities. Carbon tetrachloride shows no evidence of thermal lensing in separate measurements using fused silica as a reference. The intensity ratio given in Table II is the zero power limit of the measured ratio.

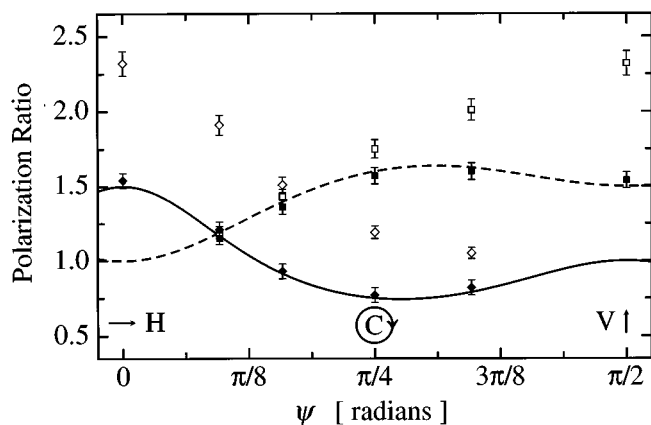


FIG. 6. Polarization ratios for carbon tetrachloride at 22 °C with irradiation at 1064 nm. The open points indicate the ratios obtained from the integrated total intensities and the filled points indicate values obtained from just the integrated Lorentzian contributions to the HRS signal. The measurements have been corrected for finite collection angle using Eqs. (6), (9), and (10). The solid line ($I_{V}^{2\omega}/I_{\psi V}^{2\omega}$) and the broken line ($I_{\psi V}^{2\omega}/I_{\psi H}^{2\omega}$) are calculated from Eqs. (6a) and (6b). The filled points follow the expected polarization dependence for a tetrahedral molecule, but the open points do not. This shows that the Lorentzian term in the spectrum correctly measures the intrinsic molecular scattering from β_{xyz} of carbon tetrachloride. In contrast, the integrated total intensity also includes large contributions due to intermolecular collisions.

large errors. Finally, when comparing HRS β values, it should be remembered that they have ultimately been calibrated making use of hyperpolarizability values taken from other nonlinear optical measurements, which may introduce other sources of systematic errors because of the use of different reference standards and techniques.^{26,27}

With this apparatus it is straightforward to obtain sufficient data for a complete polarization analysis by measuring the polarization ratios $I_{V}^{2\omega}/I_{\psi V}^{2\omega}$ and/or $I_{\psi V}^{2\omega}/I_{\psi H}^{2\omega}$ for several settings of the compensator retardation $\Gamma=2\psi$, as shown in Fig. 6 for carbon tetrachloride. In the case of CCl_4 , with its single independent component β_{xyz} , Eq. (6) predicts the polarization ratios as functions of ψ with no adjustable parameters. Figure 6 shows that the data points obtained using only the Lorentzian contribution to the spectrum are in good agreement with the calculated polarization ratios, whereas the points obtained using the entire spectrum do not agree at all. This is because intermolecular interactions account for 60% of the $I_{V}^{2\omega}$ HRS scattering from carbon tetrachloride, and only the Lorentzian component corresponds to the intrinsic

molecular hyperpolarizability.⁹ This emphasizes the need for spectral analysis in conjunction with polarization studies in order to obtain meaningful results from HRS measurements.

The present apparatus also has excellent utility in Raman scattering measurements. As shown by our measurements on the relative scattering intensity from various Raman bands of CCl_4 in the liquid and vapor phase, this setup is capable of accuracy as good or better than that of other experimental arrangements discussed in the literature.

- ¹ K. Clays, A. Persoons, and L. De Maeyer, in *Advances in Chemical Physics*, edited by M. Evans and S. Kielich (Wiley, New York, 1994), Vol. 85, p. 455.
- ² J. Zyss and I. Ledoux, *Chem. Rev.* **94**, 77 (1994).
- ³ G. J. T. Heesink, A. G. T. Ruiter, N. F. van Hulst, and B. Bölger, *Phys. Rev. Lett.* **71**, 999 (1993).
- ⁴ T. Verbiest, K. Clays, and A. Persoons, *Opt. Lett.* **18**, 525 (1993).
- ⁵ E. Chauchard, C. Combellas, E. Hendrickx, G. Mathey, C. Suba, A. Persoons, and A. Thiebault, *Chem. Phys. Lett.* **238**, 47 (1995).
- ⁶ J. Zyss, T. C. Van, C. Dhenaut, and I. Ledoux, *Chem. Phys.* **177**, 281 (1993).
- ⁷ T. Verbiest, K. Clays, C. Samyn, J. Wolff, D. Reinhoudt, and A. Persoons, *J. Am. Chem. Soc.* **116**, 9320 (1994).
- ⁸ K. Clays and A. Persoons, *Phys. Rev. Lett.* **66**, 2980 (1991).
- ⁹ P. Kaatz and D. P. Shelton, *Mol. Phys.* (in press).
- ¹⁰ M. A. Pauley, C. H. Wang, and A. K. Y. Jen, *J. Chem. Phys.* **102**, 6400 (1995).
- ¹¹ K. Clays and A. Persoons, *Rev. Sci. Instrum.* **63**, 3285 (1992).
- ¹² K. Clays and A. Persoons, *Rev. Sci. Instrum.* **65**, 2190 (1994).
- ¹³ W. J. Schmid and H. W. Schrötter, *Chem. Phys. Lett.* **45**, 502 (1977).
- ¹⁴ J. P. Neddersen, S. A. Mounter, J. M. Bostick, and C. K. Johnson, *J. Chem. Phys.* **90**, 4719 (1989).
- ¹⁵ W. P. Acker, D. H. Leach, and R. K. Chang, *Chem. Phys. Lett.* **155**, 491 (1989).
- ¹⁶ R. Bersohn, Y. H. Pao, and H. L. Frisch, *J. Chem. Phys.* **45**, 3184 (1966).
- ¹⁷ S. J. Cyvin, J. E. Rauch, and J. C. Decius, *J. Chem. Phys.* **43**, 4083 (1965).
- ¹⁸ J. Zyss, *J. Chem. Phys.* **98**, 6583 (1993).
- ¹⁹ A. Yariv and P. Yeh, *Optical Waves in Crystals* (Wiley, New York, 1984).
- ²⁰ P. D. Maker, *Phys. Rev. A* **1**, 923 (1970).
- ²¹ W. G. Rothschild, *Dynamics of Molecular Liquids* (Wiley, New York, 1984).
- ²² D. P. Shelton, *Phys. Rev. A* **42**, 2578 (1990).
- ²³ J. H. R. Clark and P. D. Mitchell, *J. Chem. Soc. Faraday Trans. II* **71**, 515 (1975).
- ²⁴ H. W. Schrötter and H. W. Klöckner, in *Raman Spectroscopy of Gases and Liquids*, edited by A. Weber (Springer, Berlin, 1979), p. 123.
- ²⁵ R. W. Terhune, P. D. Maker, and C. M. Savage, *Phys. Rev. Lett.* **14**, 681 (1965).
- ²⁶ D. M. Burland, C. A. Walsh, F. Kajzar, and C. Sentein, *J. Opt. Soc. Am. B* **8**, 2269 (1991).
- ²⁷ A. Willetts, J. E. Rice, D. M. Burland, and D. P. Shelton, *J. Chem. Phys.* **97**, 7590 (1992).